www.rericjournal.ait.ac.th

Numerical Simulation of Cylindrical Heat Pipe Using Al_2O_3-Water Nanofluid as the Working Fluid

Narong Pooyoo* and Sivanappan Kumar[#, 1]

ARTICLE INFO

Article history:
Received 13 August 2021
Received in revised form
10 July 2022
Accepted 18 July 2022

Keywords:
Al_2O_3-water nanofluid
Cylindrical heat pipe
Single phase model
Thermal conductivity
Thermal resistance

ABSTRACT

This research was aimed to study the transport and thermal characteristics in a cylindrical heat pipe using Al_2O_3-water nano fluid. Maxwell-Garnett, Hamilton and Crosser, Jang and Choi, Chon et al. and Sitprasert et al. models were used to determine the thermal conductivity. The non-Darcian transport approach was used to determine the nanofluid flow in the liquid-wick section, while the mass flow rate was used to describe the fluid flow at liquid-vapor interface. The non-linear algebraic equations from finite volume method discretization were solved by iterative segregation method and the SIMPLEC algorithm. The numerical simulation results of axial outer wall temperature, centerline pressure, velocity magnitude and nanofluid recirculation were found to be in good agreement with the values obtained for the cylindrical heat pipe operation and earlier studies. The results indicate that alumina oxide in 20 nm mixed with water can reduce the thermal resistance of the cylindrical heat pipe by 5.7% in Maxwell-Garnett model and Hamilton and Crosser model; 36% in Jang and Choi model; 3.7% in Chon et al. model; 12.1% in Sitprasert et al. model; and 21.8% in Yu and Choi model compared to pure water. The simulation result shows that the use of Al_2O_3-water nanofluid increases the effective thermal conductivity in all models. Besides, the evaporator and condenser heat transfer coefficients are found to increase in models compared to that of pure water.

1. INTRODUCTION

The use of nanofluids in heat pipes have been studied by many researchers. Maxwell-Garnett [1] developed an equation to estimate the effective medium to treat the effective transport coefficient of mixture and composites for dilute and randomly distributed components. Hamilton and Crosser [2] had derived an equation for the effective thermal conductivity considering the effect of shape of the solid particles. The Brownian motion of the nanoparticle was considered to predict the effective thermal conductivity of nanofluids by Bhattacharya *et al.* [3] and Jang and Choi [4]. Chon *et al.* [5] proposed a correlation to determine the thermal conductivity depending on temperature of Al_2O_3 nanofluid. Sitprasert *et al.* [6] analysed the thermal conductivity to nanolayer. Choi and Zhang [7] numerically simulated laminar forced convection heat transfer of Al_2O_3-water nanofluid, as a single-phase fluid. Mahmoodi [8] performed numerical simulation of Cu-water nanofluid in L-shaped cavities. The studies considered nanofluid Newtonian, laminar flow and incompressible. It was also assumed that the nanoparticles and the base fluid were in thermal equilibrium and there was no slip between them.

Many experimental, analytical, and numerical simulation studies on nanofluid heat pipes have been carried out. Do and Jang [9] studied experimentally the effect of Al_2O_3-deionized water nanofluid on a flat-shaped grooved heat pipe. Jang and Choi model [4] estimated the thermal conductivity. The viscosity of nanofluid was considered by modified Einstein model [10] with slip mechanism in nanofluids, and the density of nanofluid was estimated by mixing theory [11]. The permeability and the effective thermal conductivity of the porous layer was modeled by Kaviany [12].

Mousa [13] investigated the effect of Al_2O_3-water nanofluid concentration on the cylindrical-shaped screen mesh heat pipe. The effective physical properties were described by classical formulas in Das *et al.* [14]].

Shafahi *et al.* [15] investigated the thermal performance of a screen mesh cylindrical heat pipe using various nanofluids (Al_2O_3, CuO and TiO_2-water) with single phase model based on analytical model given by Zhu and Vafai [16]. They compared the analytical model with previous experimental results of pure water screen wick heat pipe [17] reported by Kavusi and Toghraie [18] and showed that 4% Al_2O_3 nanofluid concentration leads to decrease the temperature difference between evaporator and

*Division of Energy Human Resource Development, Department of Alternative Energy Development and Efficiency, Ministry of Energy, 17 Rama I Road, Kasatsuk Bridge, Pathumwan, Bangkok 10330 Thailand.

[#]Sustainable Energy Transition program, School of Environment, Resources and Development, Asian Institute of Technology, Klong Luang, Pathumthani 12120, Thailand.

[1] Corresponding Author:
Email: kumar@ait.ac.th.

condenser by 5% for Al_2O_3 compared to pure water, as shown in Figure 1. This two-dimensional analytical model [16] takes into account the matching condition for velocity and shear stress at the interface and non-Darcian effects for the liquid flow and shows that the coupling at the interface can be ignored. However, the Darcy law can lead to significant errors in calculating the pressure drop in the wick. The extended Darcian transport terms lead to a more accurate estimation of the pressure drop across the wick. So, for this study, the Pak and Cho model [19] was used to estimate density and Brinkman's [20] model was used to obtain the viscosity of nanofluid. The non-Darcian transport (Brinkman and Forcheiner) was used to derive the momentum equation in liquid-wick region. The effective thermal conductivity of nanofluid related to porous wick was calculated by Chi model [21] and the thermal conductivity of the nanofluid was obtained using the Yu and Choi model [22].

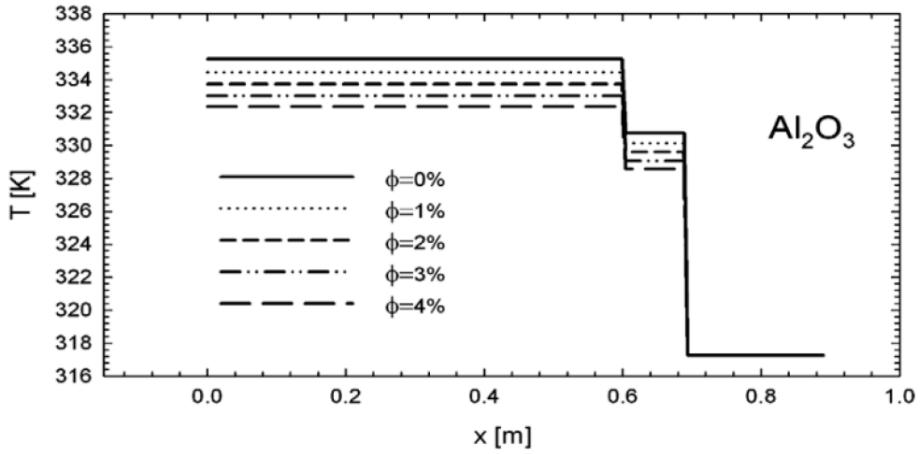

Fig. 1. Outer wall temperature distribution of Al_2O_3 nanofluids in a cylindrical heat pipe [15].

Alizad *et al.* [23] established a comprehensive analytical solution for the thermal performance and operational attributes of the startup characteristics of various nanofluids (Al_2O_3, CuO and TiO_2-water) for the flat-shaped and disk-shaped heat pipes. Dunn and Reay [24] model was used to calculate the effective thermal conductivity based on porous media.

Shafahi *et al.* [25] studied the thermal performance of rectangular and flat-shaped heat pipes using various nanofluids (Al_2O_3, CuO and TiO_2-water) by analytical solution. Gavtash *et al.* [26] simulated the effect of various nanofluids (Al_2O_3, CuO and TiO_2-water) on a cylindrical heat pipe by single phase model. Mashaei *et al.* [27] simulated a cylindrical heat pipe using Al_2O_3 nanofluid as working fluid. They found that increased velocity affected on the higher liquid flow in wick and pressure drop. Poplaski *et al.* [28] simulated cylindrical heat pipe and assumed that the liquid, Al_2O_3 nanofluid and wick structure are in local thermal equilibrium. Herrera *et al.* [29] proposed the hydrodynamical model for Al_2O_3 nanofluid simulation. Their result showed that the capillary limit occurrence is delayed by Al_2O_3-water nanofluid at 0.5% w/w optimal concentration. Maddah *et al.* [30] indicated that increasing CuO nanofluids results in the reduction of the wall temperature and the temperature difference between the evaporator and the condenser. Hassan and Harmand [31] simulated three-dimensional transient model for vapor chamber (flat heat pipe) and the effect of various nanofluids (Al_2O_3, CuO and TiO_2-water) on its performance. The 3D transient thermal model was used to calculate the vapor chamber temperature and a 3D transient hydrodynamics model was used to predict pressure and liquid velocities. The non-Darcian transport (Brinkman and Forcheiner) was used to determine liquid flow in porous media. The Maxwell model [1] was employed to predict the effective thermal conductivity of the wick based on nanofluid. An implicit finite difference method was used to solve the numerical model.

These above-mentioned studies show that nanofluid heat pipe studies are a challenge to thermal management. The numerical simulations for performance evaluation of nanofluid heat pipes use different assumptions to predict the effective thermal conductivity of nanofluids, including the nanofluid effect on thermal resistance, liquid pressure, velocity magnitude, and there are gaps in these numerical models for cylindrical heat pipes using nanofluids. To address the gaps in

- estimating and profiling the vapor pressure of cylindrical nanofluid heat pipe, and.
- analysing (and comparing) the thermodynamic properties of nano fluids using the models developed by Maxwell [1], Hamilton and Crosser [2], Jang and Choi [4], Chon *et al.* [5], Yu and Choi [20], Sitprasert *et al.* [6],

a numerical model was developed and used in a simulation study that used pure water as the working fluid in a copper cylindrical heat pipe assuming steady state laminar incompressible flow in liquid-wick and ideal gas incompressible flow in vapor section [32]. Noting the interest in Al_2O_3-water nanofluids due to its (popular) use and is one of the cheaper nanofluids, as well as due to the fact that it enhances the thermal performance and reduces the thermal resistance of heat pipes [33], it is important to estimate the thermal

conductivity of the nano fluid through a numerical model to study the axial outer wall temperature, centerline pressure and velocity magnitude using Al_2O_3-water nanofluid in a cylindrical heat pipe.

Thus, the objective of this research was to predict the axial outer wall temperature taking into consideration the thermal resistance, centerline pressure and centerline velocity magnitude using various thermal conductivity models, and to compare the nanofluid cylindrical heat pipe thermal resistance of Al_2O_3-water. Two concentrations of Al_2O_3-water nanofluid were considered (0 and 2% v/v) and the nanoparticle size is 20 nm. For the numerical simulation, the viscosity and density values were estimated using the Brinkman model [20] and Pak and Cho model [19], respectively. Maxwell-Garnett [1], Hamilton and Crosser [2], Jang and Choi [4], Chon *et al.* [5] and Sitprasert *et al.* [6] models were used to determine the thermal conductivity of nanofluids. The finite volume method was used to discretize the governing equations of non-Darcian transport (Wang and Cheng) [34] to obtain the algebraic equations. The Simi-Implicit Method Pressure Link Equation-Consistent (SIMPLEC) algorithm was used to solve the algebraic equations [35]. The results were then compared with the analytical results of Yu and Choi model [22] to estimate the effective thermal conductivity of nanofluids and pure water.

2. NANOFLUID AND ITS PROPERTIES

For this study, twenty nm Al_2O_3 mixed with water (Al_2O_3-water nanofluid) was chosen as the working fluid for the cylindrical heat pipe and this nanofluid was assumed to maintain single phase due to its ultrafine and being easily fluidized nature [36]. As described above, the Brinkman model [20] was used to determine the viscosity and Pak and Cho model [19] was used to estimate density of nanofluids. Maxwell-Garnett [1], Hamilton and Crosser [2], Jang and Choi [4], Chon *et al.* [5] and Sitprasert *et al.* [6] models were used to estimate the thermal conductivity for nanofluids.

Maxwell [1] had estimated the effective thermal conductivity of a solid-liquid mixture consisting of spherical particles. The effect of nanolayers has been studied by Sitprasert *et al.* [6] by modifying the model of Leong *et al.* [37]. This modification takes into consideration the effect of temperature on the thermal conductivity and thickness of nanolayer. The equational form of the mathematical models for viscosity, density and thermal conductivity are given in Table 1, and the results of thermal conductivity using different models in the liquid phase, vapor phase and in the wick region are shown in Table 2.

Table 1. Estimation of viscosity, density, and thermal conductivity of Al_2O_3-water nanofluids by various models.

Models	Viscosity/ Density/Thermal conductivity	
Brinkman [20]	$\mu_{nf} = \frac{\mu_{bf}}{(1-\emptyset)^{2.5}}$	(1)
Pak and Cho [19]	$\rho_{nf} = \rho_{np}\emptyset + (1-\emptyset)\rho_{bf}$	(2)
Maxwell [1]	$k_{nf} = k_{bf}\left[\frac{(1-\emptyset)(k_{np}+2k_{bf}) + 3\emptyset k_{np}}{(1-\emptyset)(k_{np}+2k_{bf}) + 3\emptyset k_{bf}}\right]$	(3)
Hamilton and Crosser [2]	$k_{nf} = \frac{k_{bf}\left[(k_{np}+(n-1)k_{bf} + (n-1)\emptyset(k_{np}-k_{bf})\right]}{k_{np}+(n-1)k_{bf} - \emptyset(k_{np}-k_{bf})}$	(4)
Jang and Choi [4]	$k_{nf} = \emptyset k_{np} + (1-\emptyset)k_{bf} + 3C_1\frac{d_{bf}}{d_{np}}k_{bf}Re_d^2 Pr_{bf}\emptyset$	(5)
Chon *et al.* [5]	$\frac{k_{nf}}{k_{bf}} = 1 + 64.7\emptyset^{0.7460}\left(\frac{d_{bf}}{d_{np}}\right)^{0.3690}\left(\frac{k_{np}}{k_{bf}}\right)^{0.7476} Pr^{0.9955}Re^{1.2321}$	(6)
Sitprasert *et al.* [6]	$\frac{k_{nf}}{} = \frac{(k_{np}-k_{lr})\emptyset k_{lr}\left[2{\beta_1}^3 - {\beta_0}^3 + 1\right] + (k_{np}\pm 2k_{lr})\beta_1^3\left[\emptyset{\beta_0}^3(k_{lr}-k_{bf}) + k_{bf}\right]}{\beta_1^3(k_{np}\pm 2k_{lr})(k_{np}-k_{lr})\emptyset\left[\beta_1^3 \pm {\beta_0}^3 - 1\right]}$	(7)

Table 2. Thermal conductivity estimation of Al_2O_3-water nanofluid in vapour phase, liquid phase and wick by various models.

Description and model used	Symbol and unit	Value
Thermal conductivity of nanofluid in vapor phase (Maxwell-Garnett model)	$k_{nf,v}$, W/m.K	0.0236
Thermal conductivity of nanofluid in vapor phase (Hamilton-Crosser model)	$k_{nf,v}$, W/m.K	0.0236
Thermal conductivity of nanofluid in vapor phase (Jang-Choi model)	$k_{nf,v}$, W/m.K	0.742
Thermal conductivity of nanofluid in vapor phase (Chon *et al.* model)	$k_{nf,v}$, W/m.K	0.162
Thermal conductivity of nanofluid in vapor phase (Sitprasert model)	$k_{nf,v}$, W/m.K	0.159
Thermal conductivity of nanofluid in liquid phase (Maxwell-Garnett model)	$k_{nf,l}$, W/m.K	0.695
Thermal conductivity of nanofluid in liquid phase (Hamilton-Crosser model)	$k_{nf,l}$, W/m.K	0.695
Thermal conductivity of nanofluid in liquid phase (Jang-Choi model)	$k_{nf,l}$, W/m.K	1.364
Thermal conductivity of nanofluid in liquid phase (Chon *et al.* model)	$k_{nf,l}$, W/m.K	0.657
Thermal conductivity of nanofluid in liquid phase (Sitprasert model)	$k_{nf,v}$, W/m.K	0.791
The effective thermal conductivity of wick (Sitprasert model)	k_{eff}, W/m.K	0.990
The effective thermal conductivity of wick (Jang-Choi model)	k_{eff}, W/m.K	1.626
The effective thermal conductivity of wick (Chon *et al.* model)	k_{eff}, W/m.K	0.841
The effective thermal conductivity of wick (Hamilton-Crosser model)	k_{eff}, W/m.K	0.883
The effective thermal conductivity of wick (Maxwell model)	k_{eff}, W/m.K	0.883

3 GOVERNING EQUATIONS

The governing equations and related equations are given in cylindrical coordinates and velocity components in r, θ, z directions, respectively:

3.1 Liquid-wick Region

The nanofluid flow through porous wick (liquid-wick region) also uses the assumptions presented earlier [38], [48], [50]. They create compact vector notation form, as follows [29]:

$$\nabla.\left(\rho_{nf}\varepsilon\vec{V}\vec{V}\right) = -\varepsilon\nabla P + \nabla.(\varepsilon\tau) - \frac{\mu_{nf}\varepsilon^2\vec{V}}{K} - \frac{\varepsilon^3\rho_{nf}C_F}{\sqrt{K}}|\vec{V}|\vec{V} \quad (8)$$

The C_F can be calculated from [51],

$$C_F = \frac{1.75}{\sqrt{150\varepsilon^3}} \quad (9)$$

The permeability of screen wick structures is given by the following equation [21].

$$\frac{d_w^2\varepsilon^3}{122(1-\varepsilon)^2} \quad (10)$$

$$\varepsilon = 1 - \left(\frac{1.05\pi N d_w}{4}\right) \quad (10.a)$$

3.2 Liquid-vapor Interface

The mass balance equation in the r - direction at the liquid-vapor interface yields:

$$\rho_{nf,l}A_i v_{nf,l} = \rho_{nf,v}A_i v_{nf,v} \quad (11)$$

The blowing velocity and suction velocity at liquid-vapor interface can be calculated from the following equations [16], [39]-[45]:

$$Q_i^{\cdot} = m_{nf,i}^{\cdot}h_{fg,nf} = \rho_{nf,v}A_i V_{nf,i}h_{fg,nf} \quad (12)$$

$$V_{i,e} = -\frac{\dot{Q}_{i,e}}{2\pi R_i L_e \rho_{nf,v}h_{fg,nf}} \quad (13)$$

$$V_{i,a} = 0 \quad (14)$$

$$V_{i,c} = +\frac{\dot{Q}_{i,c}}{2\pi R_i L_c \rho_{nf,v}h_{fg,nf}} \quad (15)$$

The mass flow rate per radian applies for the inlet boundary condition at liquid-vapor interface for evaporator, adiabatic section and condenser, as follows:

$$m_{i,e}^{\cdot} = -[\rho_{nf,v}(2\pi R_i L_e)V_{i,e}]/2\pi \quad (16)$$

$$m_{i,a}^{\cdot} = 0 \quad (17)$$

$$m_{i,c}^{\cdot} = +[\rho_{nf,v}(2\pi R_i L_c)V_{i,c}]/2\pi \quad (18)$$

The negative sign refers to outflow liquid-wick region and the positive sign for inflow liquid-wick region.

3.3 Vapor Region

The generalized Navier-Stokes equations to simulate the vapor flow inside vapor region uses the previously noted assumptions [38], [46]-[50]

These assumptions help to formulate the generalized Navier-Stoke equations in compact vector notation form in the vapor region, as follows [51], [53]:

$$\nabla.\left(\rho_{nf,v}\vec{V}\vec{V}\right) = -\nabla P + \nabla.(\tau) \quad (19)$$

3.4 Total Enthalpy Equation

The nanofluid cylindrical heat pipe uses total enthalpy equation in liquid-wick region, vapor region and cylindrical heat pipe container, as follows:

3.4.1 Liquid-wick Region

The total enthalpy equation in liquid-wick region used to obtain the temperature profile inside liquid-wick region of cylindrical heat pipe is presented in compact vector notation, as follows [51], [53]:

$$\nabla.\left(\rho_{nf,l}\varepsilon\vec{V}h_0\right) = \nabla.\left(k_{eff}\Delta T\right) + (\varepsilon\tau):\nabla\vec{V} + \varepsilon\frac{\partial p}{\partial t} + S_h \tag{20}$$

$$h_0 = i + \frac{p}{\rho_{nf,l}} + \frac{1}{2}(u^2 + v^2 + w^2) \tag{20.a}$$

The effective thermal conductivity of screen wick and source terms can be calculated by the following equation [54], [42].

$$k_{eff} = \frac{k_{nf}\left[\left(k_{nf} + k_s\right) - (1-\varepsilon)\left(k_{nf} - k_s\right)\right]}{\left[\left(k_{nf} + k_s\right) + (1-\varepsilon)\left(k_{nf} - k_s\right)\right]} \tag{21}$$

$$S_e = -\frac{\dot{Q}_{i,e}}{\pi((R_i + t_w)^2 - {R_i}^2)L_e} \tag{22}$$

$$S_a = 0 \tag{23}$$

$$S_c = +\frac{\dot{Q}_{i,c}}{\pi((R_i + t_w)^2 - {R_i}^2)L_c} \tag{24}$$

The source term of evaporation has a negative sign, referring to the heat loss in evaporator liquid-wick region, and the source term of condensation has a positive sign, referring to heat received in condenser liquid-wick region.

3.4.2 Vapor Region

The total enthalpy equation used to obtain temperature profile inside vapor core of cylindrical heat pipe, is given as [51]-[53]:

$$\nabla.\left(\rho_{nf,v}\vec{V}h_0\right) = \nabla.\left(k_{nf,v}\Delta T\right) + (\tau):\nabla\vec{V} + \frac{\partial p}{\partial t} \tag{25}$$

3.4.3 Nanofluid Cylindrical Heat Pipe Container

This study uses the total enthalpy equation to indicate heat transfer at the container of nanofluid cylindrical heat pipe. The total enthalpy equation is given by the following equation [51]-[53]:

$$\nabla.\left(k_s\Delta T\right) = 0 \tag{26}$$

4. COMPUTATIONAL DOMAINS AND CALCULATION PROCEDURE

The geometry of the water-alumina oxide cylindrical heat pipe used in this study has the dimensions shown in Figure 2a. The three-dimensional framework of the one segment geometry in *r, θ, z* coordinates consist of evaporator (A), adiabatic section (B) and condenser (C) and is shown in Figure 2b. The grid for a portion of the segment in three dimensions is generated by two-dimensional grid extrusion method using the CFD-GEOM program and shown in Figure 2c. The generated grid in r, θ, z coordinates is quadrilateral, and the number of total nodes is 1,244,400. The grid points are 38 × 30 × 1,360 in the radial, circumferential, axial direction, respectively.

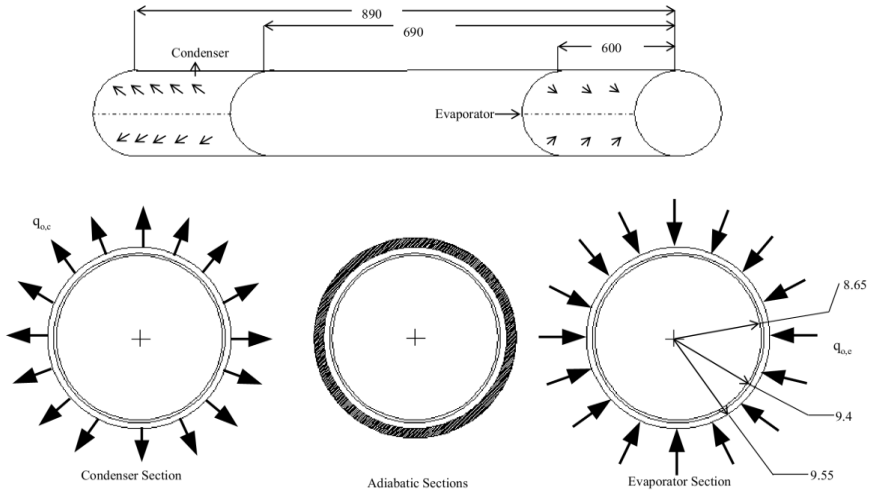

(a) Cylindrical heat pipe model used for the numerical simulation [15], [16].

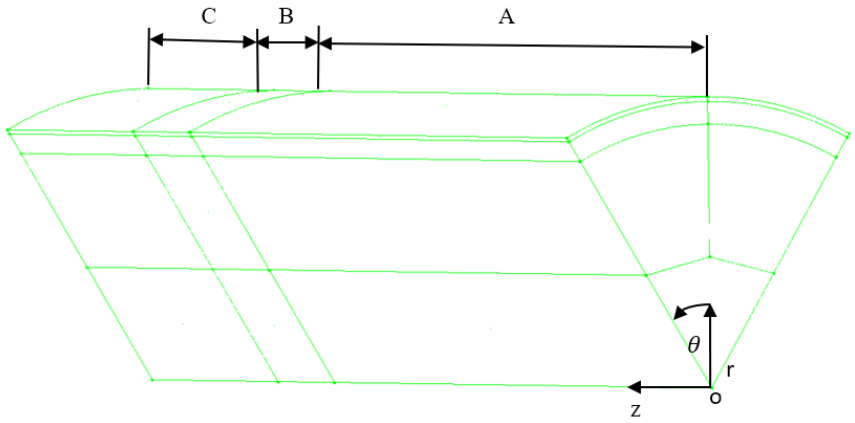

(b) 3D one segment cylindrical heat pipe geometry in *r,θ,z* coordinates.

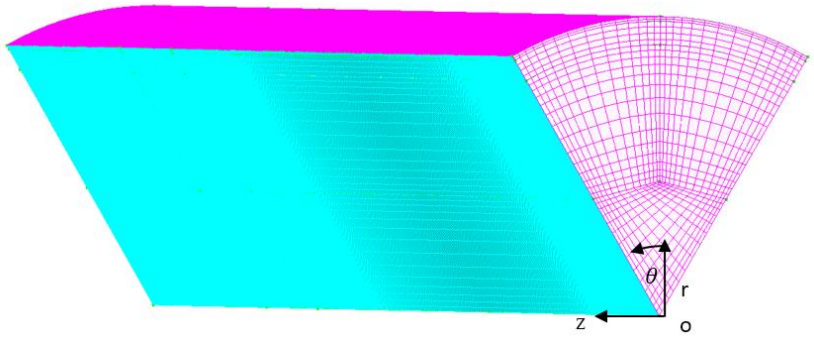

(c) 3D one segment cylindrical heat pipe grid in r, θ, z coordinates.

Fig. 2. The dimensions and structure of the cylindrical heat pipe model used for the numerical simulation [15], [16].

The flow and heat transfer of nanofluid cylindrical heat pipes are obtained by the finite volume method. This uses the finite different equations, which has both non-linear and linear equation forms in 3D steady state, laminar flow. An iterative segregation and the SIMPLEC algorithm were employed to solve the non-linear algebraic equations. The conjugate gradient squared (CGS) with enthalpy and velocity preconditioner and algebraic multigrid (AMG) solver were applied to solve the linear equation at the end of the previous iteration for pressure correction. The number of iterations and the details convergence results for each thermal conductivity models are given in Table 3. The table also shows that the residual plot for enthalpy, velocity and pressure component is four orders of magnitude drop from the peak residual. The mass flow summary is small relative to the mass incoming value as fifteen orders of magnitude and total heat imbalance is not more than 1% of heat input. These results guarantee that grid system, problem definition and the numerical solution for this analysis is valid.

5. NUMERICAL METHOD AND BOUNDARY CONDITIONS

The nanofluid cylindrical heat pipe numerical solution is solved by finite volume method. The finite volume method is used to discretize the governing equations of non-Darcian transport (Wang and Cheng) [31] to obtain the algebraic equations. The details of boundary conditions, working fluid properties and finite volume method are presented as follows:

Table 3. Summary of convergence results and the residual plots of the various models.

Descriptions	Pure water	Nanofluid (Maxwell-Garnett)	Nanofluid (Hamilton and Crosser)	Nanofluid (Jang and Choi)	Nanofluid (Chon *et al.*)	Nanofluid (Sitprasert *et al.*)
Convergence	9,530 iterations	11,770 iterations	11,770 iterations	6,616 iterations	12,177 iterations	10,798 iterations
Residual plot for enthalpy (Absolute error in the solution of a enthalpy)	1E-004	1E-004	1E-004	1E-004	1E-004	1E-004
Residual plot for velocity (Absolute error in the solution of a velocity)	1E-004	1E-004	1E-004	1E-004	1E-004	1E-004
Residual plot for pressure (Absolute error in the solution of a pressure)	1E-004	1E-004	1E-004	1E-004	1E-004	1E-004
Inflow-outflow imbalance	1.35E-020	6.78E-021	6.78E-021	6.78E-021	6.78E-021	6.78E-021
Total heat imbalance	Less than 1% of heat input	Less than 1% of heat input	Less than 1% of heat input	Less than 1% of heat input	Less than 1% of heat input	Less than 1% of heat input

5.1 Boundary Conditions and Working Fluid Properties

The CFD-ACE+ solver software is used to obtain boundary conditions and nanofluid properties. The boundary conditions for the model are given in Figure 3 and the working fluid properties (Al_2O_3-water nanofluid) are given in Table 4. These include nanofluid diameter, density, thermal conductivity, and specific heat, and the nano fluid density, specific heat and viscosity in liquid and vapour phase.

Figure 3a shows the outer wall boundary condition, in both 2 and 3D domains. The simulation assumes a 455W [16] uniform heat input at the evaporator ($+Q_e$), representing the heat generated by an electronic device. The convection heat transfer in the condenser ($-Q_c$) can be calculated from mass flow rate, cooling water entering temperature and the convective heat transfer coefficient [16]. The adiabatic wall and zero static pressure boundary conditions are the input to the evaporator end cap (A), while the opposite end cap has only the adiabatic wall boundary condition. The symmetrical boundary condition is assigned to the surface (B) and its opposite side including centerline (C).

Figure 3b shows, the container (A), liquid-wick region (B) and vapor region (C) boundary conditions:

The wall-liquid interface boundary condition is assigned to conjugate heat transfer problem with no-slip condition. The liquid-vapor interface boundary condition is assigned to the outflow mass flow rate ($-\dot{m}_{i,e}$) and inflow mass flow rate per radian ($+\dot{m}_{i,c}$) with no-slip condition.

The screen wick characteristics and other data shown in Table 5 are inputs to CFD-ACE+.

Table 4. Summary of nanofluid properties used for the simulation.

Descriptions	Symbol and unit	Value
Nanoparticle diameter	d_p , nm	20
Nanoparticle density	ρ_p , kg/m^3	3,880
Nanoparticle thermal conductivity	k_p , W/m^2.K	36
Nanoparticle specific heat	$C_{p,p}$, J/kg.K	773
Nanofluid density (liquid phase)	ρ_{nf} , kg/m^3	1,038.35
Nanofluid specific heat (liquid phase)	$C_{p,nf,l}$, J/kg.K	4,118.72
Nanofluid viscosity (liquid phase)	$\mu_{nf,l}$, Pa.s	0.000453
Nanofluid density (vapor phase)	$\rho_{nf,v}$, kg/m^3	77.759
Nanofluid specific heat (vapor phase)	$C_{p,nf,v}$, J/kg.K	1,472.72
Nanofluid viscosity (vapor phase)	$\mu_{nf,v}$, Pa.s	1.118E-005

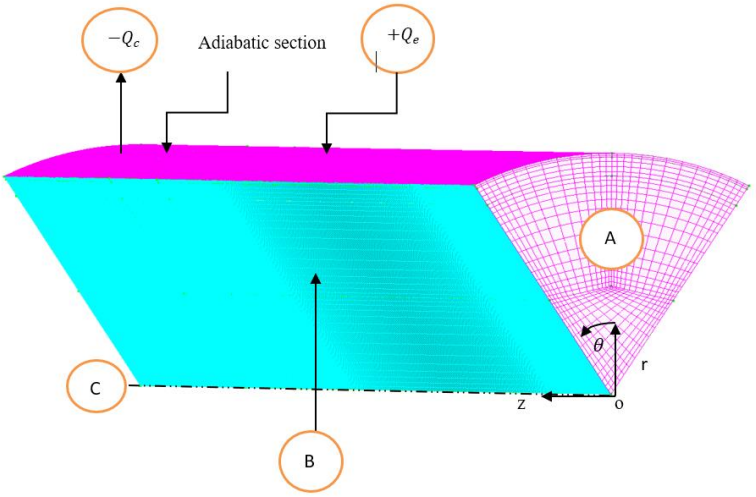

(a) Boundary conditions in the 3D computation domains.

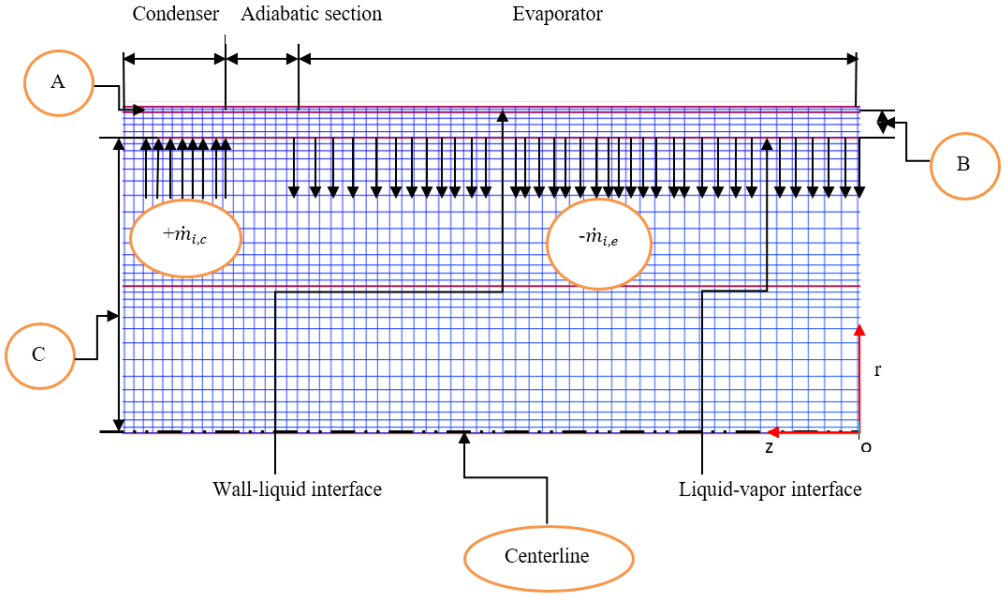

(b) Boundary conditions in the 2D computation domains.

Fig. 3. Boundary conditions of the cylindrical heat pipe model shown in different computation domains.

Table 5. The Al_2O_3-water nanofluid working fluid properties and characteristics of liquid-saturated wick structure [19], [20].

Descriptions	Symbol and unit	Value
Saturation pressure (base fluid)	P_s, Pa	24,400
Saturation temperature (base fluid)	T_s, K	338.15
Latent heat (base fluid)	h_{fg}, J/kg	2,496,025
Vapor density (base fluid)	ρ_v, kg/m^3	0.162
Vapor dynamic viscosity (base fluid)	μ_v, Pa.s	0.00001063
Specific heat for vapor (base fluid)	C_v, J/kg.K	1,850
Thermal conductivity (base fluid)	k_v, W/m.K	0.0222
Liquid density (base fluid)	ρ_l, kg/m^3	980.354
Liquid dynamic viscosity (base fluid)	μ_l, Pa.s	0.0004306
Specific heat for liquid (base fluid)	C_l, J/kg.K	4,186
Thermal conductivity (base fluid)	k_l, W/m.K	0.657
Wick porosity	ε, -	0.9
Wick permeability	K, m^2	1.5E-009

6. RESULTS AND DISCUSSIONS

The numerical simulation was done in two phases. Firstly, the simulation was carried out using water as the fluid and the observations of the simulation results were compared with experimental results of a similar set up. This was to validate the numerical procedure and the assumptions used. Accordingly, the simulation results obtained from this study on the outer wall temperature using water was compared and validated with previous experimental results in [17] and reported by Kavusi and Toghraie [18], as shown in Figure 4.

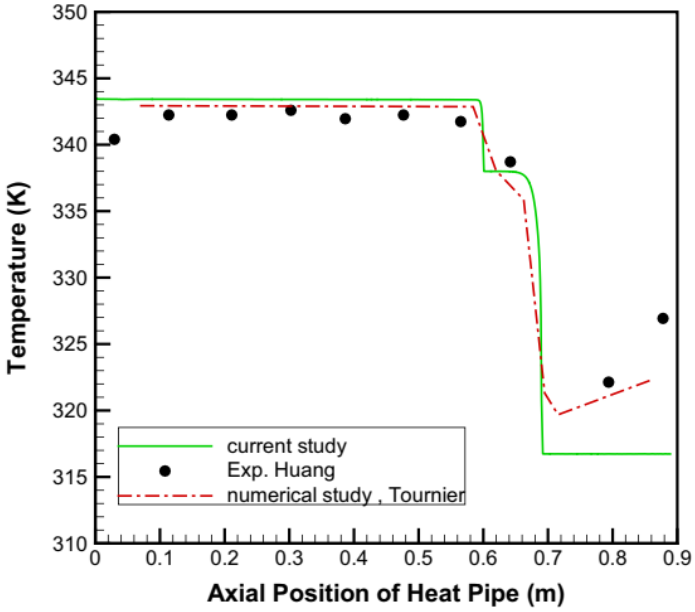

Fig. 4. Outer wall temperature profile along the axial direction of a cylindrical heat pipe: Experimental results of pure water [17] given by Kavusi and Toghraie [18] compared with the simulation results of the present work.

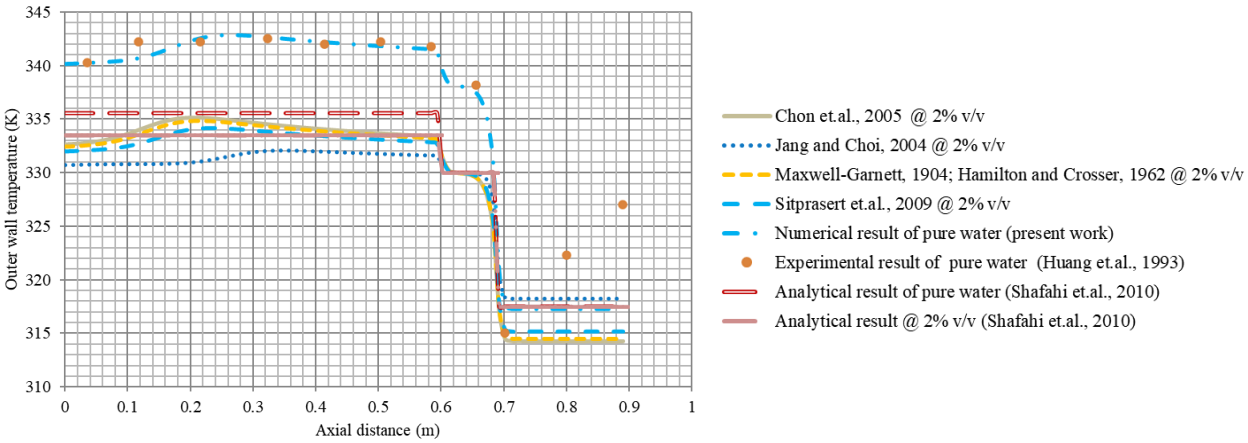

Fig. 5. Outer wall temperature distribution of a cylindrical heat pipe: Simulation results of Al_2O_3–water nanofluid using different models and pure water.

Table 6. Summary of the outer wall temperature distribution studies.

Description	Pure water experimental results of Huang *et al.*, 1993 [17]	Pure water numerical simulation results (this study)	CuO nanofluid @ 2% v/v reported by Shafahi *et al.*, 2010 [15]	Al_2O_3 nanofluid @ 2% v/v (this study)					
				Maxwell-Garnett [1]	Hamilton and Crosser [2]	Jang and Choi [4]	Chon *et al.* [5]	Sitprasert *et al.* [6]	Yu and Choi [20] reported by Shafahi *et al.*, 2010 [15]
The effective thermal conductivity (W/m. K)	38,003.97	31,747.53	47,427.72	40,301.27	40,301.27	59,375.16 (56.2% Max. compared with [17])	39,482.97 (3.9% Min. compared with [17])	43,211.92	48,613.41
Evaporator heat transfer coefficient (W/m. K)	3,239.2	3,324.4	N/A	3,324.4	3,324.4	9,023.5	3,158.2	3,947.8	3,609.4
Condenser heat transfer coefficient (W/m. K)	-2,287.2	-1,830.9	N/A	-2,445.1	-2,445.1	-3,239.2	-2413.9	-2,560.7	-3031.9
Thermal resistance (K/W)	0.045	0.054	0.036	0.042	0.042	0.029	0.043	0.040	0.035
Thermal resistance difference compared with pure water experimental results of Huang *et al.*, 1993 [17] (%)	Compared	19.7	-19.9	-5.7	-5.7	-36.0 (Max.)	-3.7 (Min.)	-12.1	-21.8

Table 6. Summary of the outer wall temperature distribution studies (Continue).

Description	Pure water experimental results of Huang *et al.*, 1993 [17]	Pure water numerical simulation results (this study)	CuO nanofluid @ 2% v/v reported by Shafahi *et al.*, 2010 [15]	Al_2O_3 nanofluid @ 2% v/v (this study)					
				Maxwell - Garnett [1]	Hamilton and Crosser [2]	Jang and Choi [4]	Chon *et al.* [5]	Sitprasert *et al.* [6]	Yu and Choi [20] reported by Shafahi *et al.*, 2010 [15]
Thermal resistance difference compared with pure water numerical simulation results of this study (%)	-16.5	Compared	-33.1	-21.2	-21.2	-46.5	-19.6	-26.5	-34.7
Thermal resistance difference compared with CuO nanofluid analytical model [15] (%)	24.8	49.4	Compared	17.7	17.7	-20.1	20.1	9.8	-2.4
The effective thermal conductivity difference compared with CuO nanofluid analytical model [15] (%)	-19.9	-33.1	Compared	-15	-15	25.2	-16.8	-8.9	2.5
Evaporator heat transfer coefficient difference (heat flux @ 12,632 W/m^2) compared with pure water experimental results of Huang *et al.*, 1993 [17] (%)	Compared	2.6	N/A	2.6	2.6	178.6	-2.5	21.9	11.4
Condenser heat transfer coefficient difference (heat flux @ 37,898.6 W/m2) compared with pure water experimental results of Huang *et al.*, 1993 [17] (%)	Compared	-19.97	N/A	6.9	6.9	41.6	5.5	11.9	32.5

N/A: Not available

6.1 The Outer Wall Temperature Distribution

Then, the study was conducted using Al_2O_3–water nanofluid. A numerical simulation study for Al_2O_3 with water nano fluid cylindrical heat pipe considering non-Darcian transport was conducted by assuming a heat input of 455W [15],[16] to the evaporator of the heat pipe. The results of the simulation in terms of the wall temperature, vapor temperature and pressure, liquid pressure drop, and velocity distribution are discussed in this section.

The outer wall temperature using nanofluid and pure water obtained has been compared with analytical and experimental observations [15],[16]-[18], and is shown in Figure 5 and Table 6 The simulation results shows very good agreement with the experimental results using water [16], [17], and in good agreement with analytical results using nanofluids [15]. In addition, the calculation using all the effective thermal conductivity models of nanofluid has lower temperature distribution compared to that of pure water. The heat pipe performance in terms of thermal resistance reductions have been compared to pure water using the thermal conductivity models of Maxwell, Hamilton and Crosser, Jang and Choi, Chon *et al.*, Sitprasert *et al.*, and Yu and Choi model reported by M. Shafahi *et al.* [15]. The thermal resistance reductions were observed to be 5.7%, 5.7%, 36%, 3.7%, 12.1% and 21.8%, respectively. Following the results obtained for the study on water, investigations of the heat transfer performance of copper cylindrical heat pipe using Al_2O_3–water nanofluid with 2% v/v showed that the thermal resistance of heat pipe decreases with the use of Al_2O_3–water nanofluid by 36% (maximum) in Jang and Choi model to a minimum of 3.7% in Chon *et al.* model compared with pure water. This decrease was due to the effective thermal conductivity increase by 56.2% (maximum) in Jang and Choi model to 3.9% minimum in Chon *et al.* model compared with pure water as 38,003.97 W/m. K. The thermal resistance using Al_2O_3–water nanofluid is less compared to CuO-water by 20.1% in Jang and Choi *et al.* model, 2.4% Yu and Choi model, and it is more than 17.7% in Maxwell-Garnett model, 20.1% in Chon model, and 9.8% in Sitprasert *et al.* model.

The effective thermal conductivity of cylindrical heat pipe using Al_2O_3–water nanofluid is more by using CuO-water by 25.2% in Jang and Choi model, 2.5% in Yu and Choi model, and it is less than 15% in Maxwell-Garnett model, 16.8% in Chon *et al.* model, and 8.9% in Sitprasert model.

It is observed that the evaporator and condenser heat transfer coefficients are increased due to the increase of the effective thermal conductivity and the reduction of the temperature difference between the wall temperature and the centerline vapor temperature of evaporator and condenser section of cylindrical heat pipe. The evaporator heat transfer coefficient is more than the condenser heat transfer coefficient. This is because the heat flux at evaporator (12,632.9 W/m^2) is less than the heat flux at condenser (37,898.6 W/m^2). In addition, the evaporator and condenser heat transfer coefficient of Al_2O_3–water nanofluid are increased by 11.4% (minimum) in Yu and Choi model to 178.6% (maximum) in Jang and Choi model compared with pure water.

6.2 The Centerline Vapor Temperature Distribution

The simulation was done to profile the centerline vapor temperature distribution along the axial distance and was done using two working fluids – water and Al_2O_3–water nanofluid. The results are shown in Figure 6.

The centerline vapor temperature distribution along the axial distance using water is in very good agreement with experimental observations [16]. Also, the centerline vapor temperature considering the effective thermal conductivity of nanofluids is lower than that of pure water because the operating and evaporator temperature reduction leads to the decrease of vapor temperature [55], and its temperature is constant at 330.15 K.

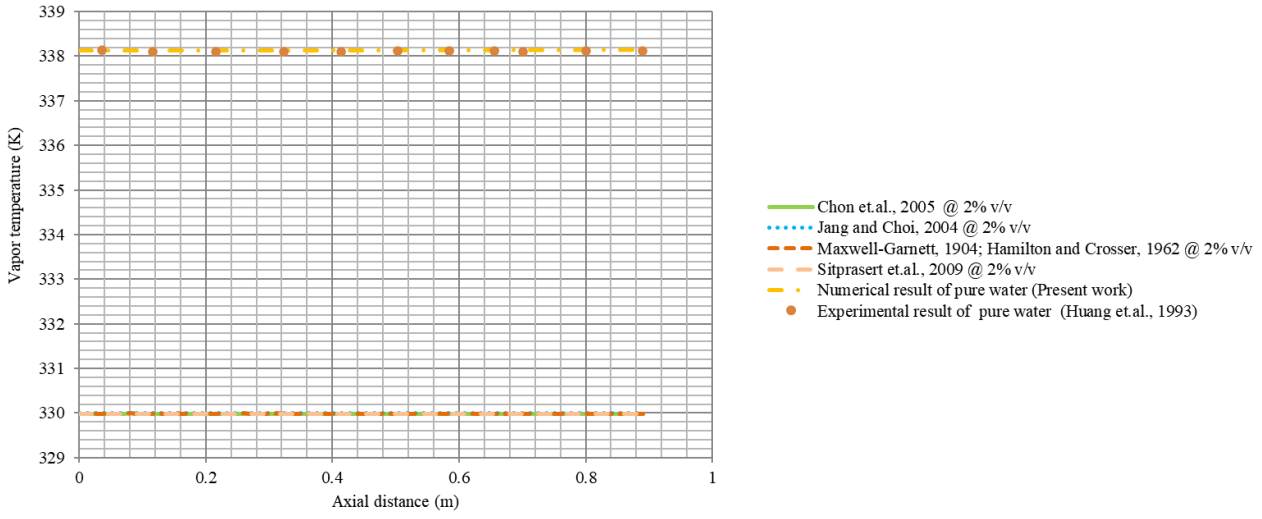

Fig. 6. Centerline vapor temperature distribution in a cylindrical heat pipe: Simulation results of Al_2O_3–water nanofluid using different models and pure water.

6.3 Liquid Pressure Drop and Velocity

The liquid pressure and velocity using nanofluid and pure water obtained from this work was compared with the previous numerical results, and analytical studies [15], [16], and the results are shown in Figure 7.

The liquid pressure drop using pure water and Al_2O_3–water nanofluid in the liquid-wick region sharply decreases from condenser through adiabatic to evaporator sections as shown in Figure 7a. The porous media causes that liquid pressure drop is much higher than the vapor pressure drop. This result is in good agreement with the previous studies [15], [16].

The liquid pressure distribution shown in Figure 7a affects the velocity magnitude sharply and decreases in the condenser due to condensation, and this decrease is nearly uniform at the adiabatic section due to small temperature difference, and sharply increases at evaporator zone due to evaporation. This phenomenon is due to energy conservation and the change from potential energy to kinetic energy. Figure 7b shows the liquid velocity magnitude of nanofluid is similar to that of pure water. These results are also in good agreement with earlier studies [16], [22].

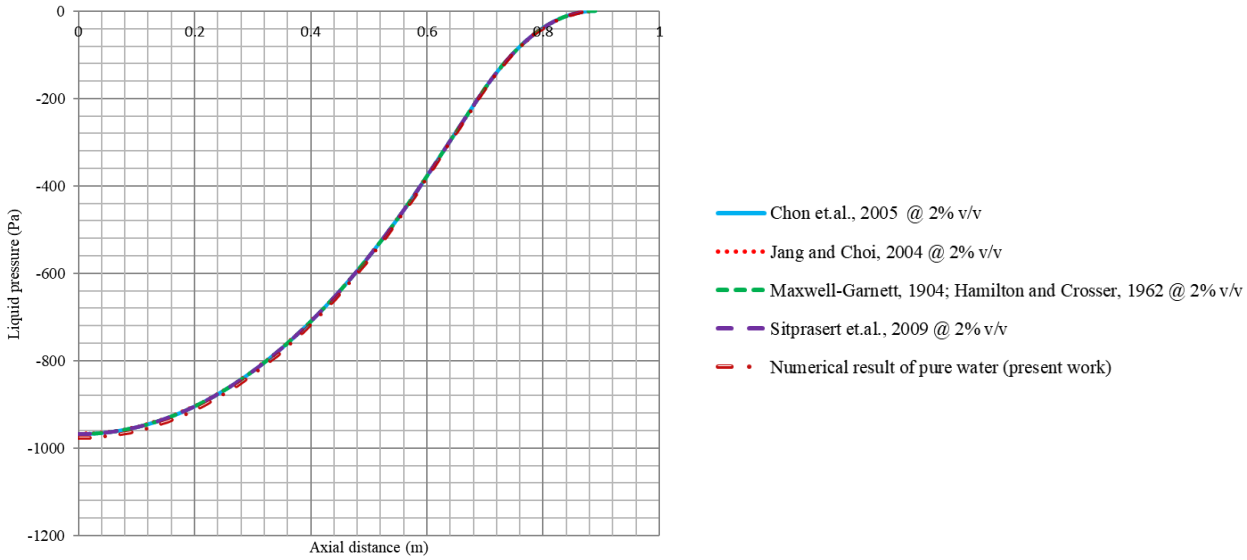

(a) Comparison of liquid pressure profile of Al_2O_3–water nanofluid and pure water.

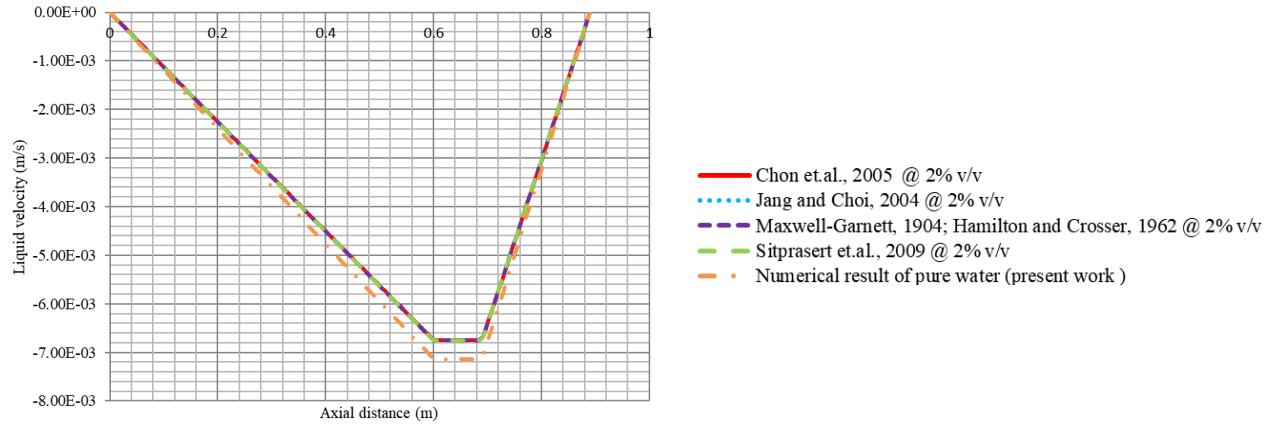

(b) Comparison of liquid velocity trend of Al_2O_3–water nanofluid and pure water.

Fig. 7. The liquid pressure and liquid velocity distribution along the axial direction of cylindrical heat pipe using Al_2O_3–water nanofluid (using different models) and pure water.

6.4 The Centerline Vapor Pressure and Velocity Distribution

The centerline vapor pressure distribution using water as working fluid shows very good agreement with earlier experimental results [16]. This result indicates that the effective thermal conductivity of nanofluid models is higher than that of pure water.

The rate of vaporization in the evaporator and condensation is assumed to be uniform. This produces a linearly increasing centerline velocity magnitude in the evaporator, and a linearly decreasing centerline velocity magnitude in the condenser, when considering pure water and nanofluids. This is shown in Figure 8a-c.

Figure 8a shows the vapor pressure for the effective thermal conductivity of nanofluid model have higher values when using pure water. The vapor pressure is found to be constant at 24,495 Pa, which is due to the incompressible flow occurring along the vapor flow path. These results show good agreement with earlier study [16].

Figure 8b shows that the saturation pressure is 24,494 Pa at the vapor region. The contour of pressure shows no difference at vapor zone and at centerline in r-z plane. As shown in Figure 8c, the temperature of water vapor at vapor zone and at centerline is constant at 330.15 K (57°C).

Figure 8d-e shows that the centerline velocity magnitude of nanofluid is much less than that of pure water. This result relates to centerline pressure distribution shown in Figure 8a. That is, the velocity magnitude increases when pressure is decreased, and the velocity magnitude decreases when pressure is increased. This phenomenon is in good agreement with earlier numerical results [16], [22].

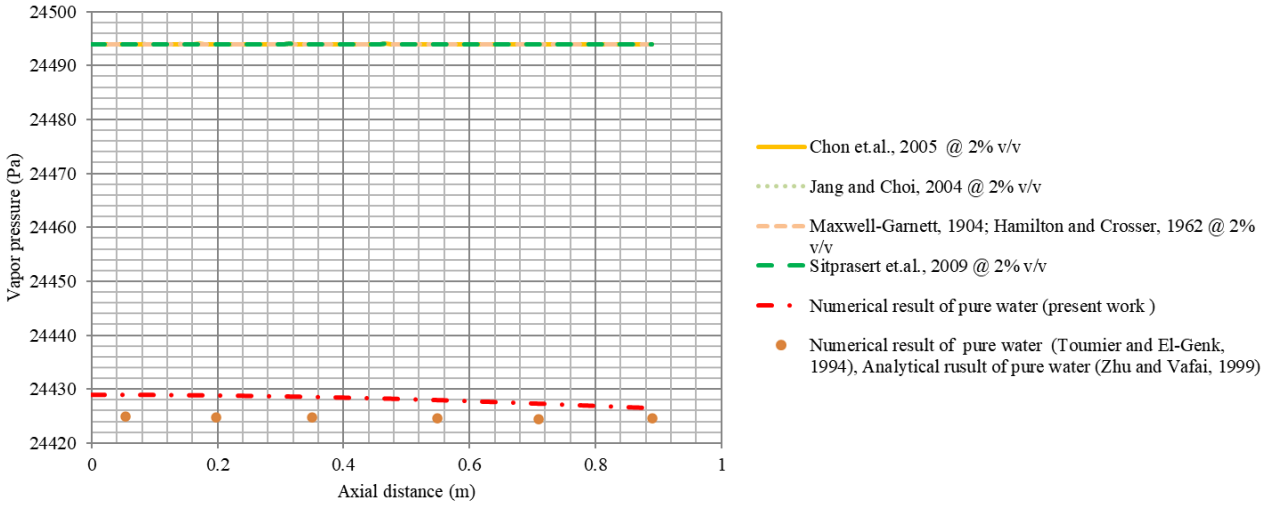

(a) The centerline pressure of Al_2O_3–water nanofluid and pure water.

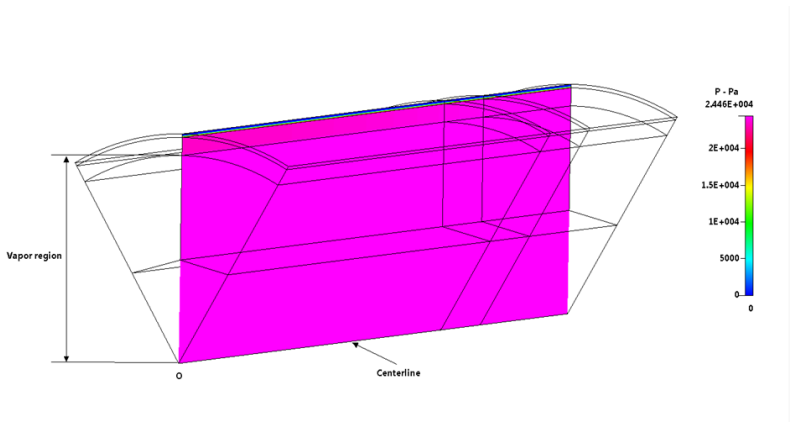

(b) The contour of pressure using pure water in r-z plane.

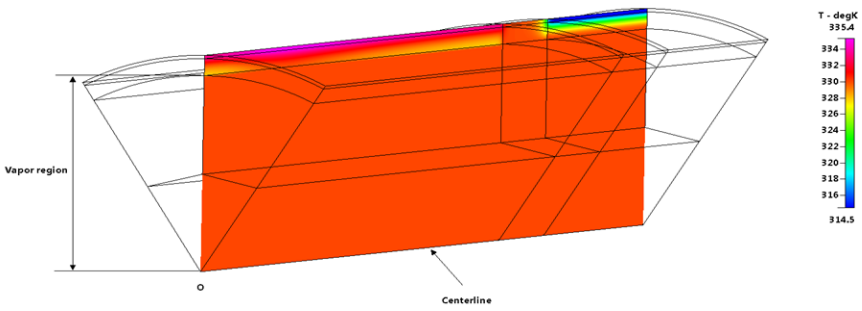

(c) The contour of temperature using pure water in r-z plane.

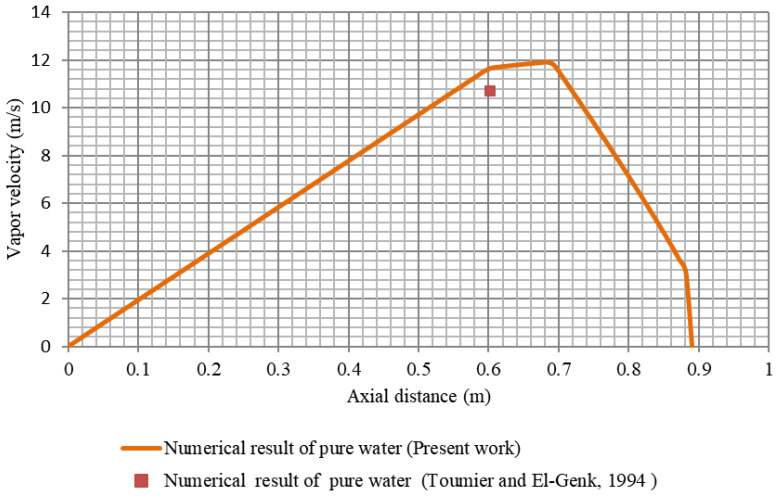

(d) The centerline vapor velocity of pure water.

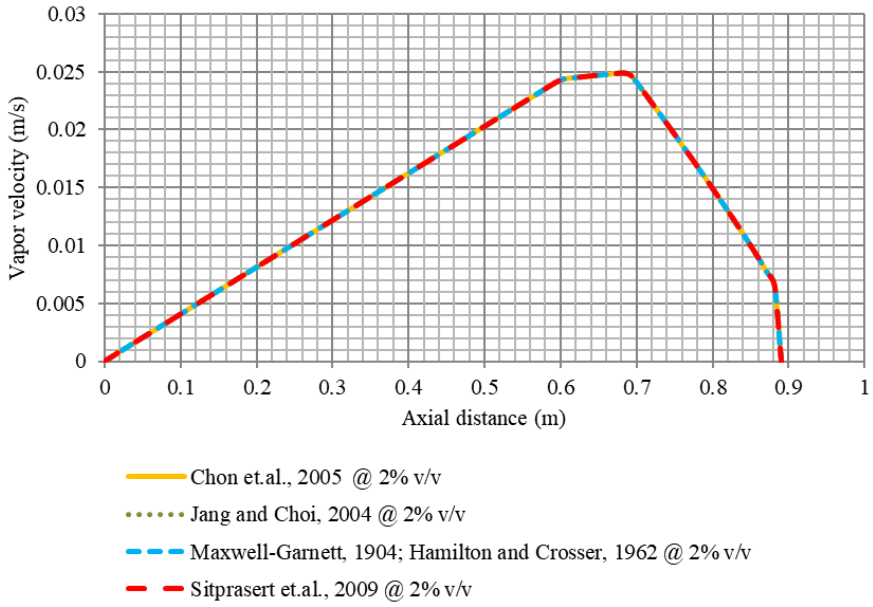

(e) The centerline vapor velocity of Al_2O_3–water nanofluid.

Fig. 8. The centerline vapor pressure and velocity distribution of Al_2O_3–water nanofluid and pure water in a cylindrical heat pipe.

6.5 The Velocity Contour

The contour of velocity magnitude obtained from numerical simulation for the two cases - Al_2O_3–water nanofluid and pure water - is shown in Figures 9a-c.

The contours of velocity magnitude in the symmetry plane and in the r-z plane using Al_2O_3–water nanofluid (Maxwell model) and pure water is similar to that of pure water at the different velocity magnitudes. The highest velocity magnitude occurs near the centerline of cylindrical heat pipes in the adiabatic section. The velocity magnitude is found to be linearly increasing at the evaporator, and to be linearly decreasing at the condenser. The velocity magnitude at the adiabatic section increases from near wall volume condition to centerline boundary condition. The zero-velocity magnitude occurs at the wall volume condition and at the end caps of the cylindrical heat pipes.

7. CONCLUSIONS

A model for the nanofluid cylindrical heat pipe was developed considering flow and thermal field in nanofluid as single phase incorporated with the non-Darcian transport [32]. The Brinkman and Pak and Cho model were used to obtain the viscosity and density of nanofluids, respectively. The Maxwell-Garnett [5], Hamilton and Crosser [6], Jang and Choi [8], Chon *et al.* [9] and Sitprasert *et al.* [6] models were used to estimate the thermal conductivity in nanofluids.

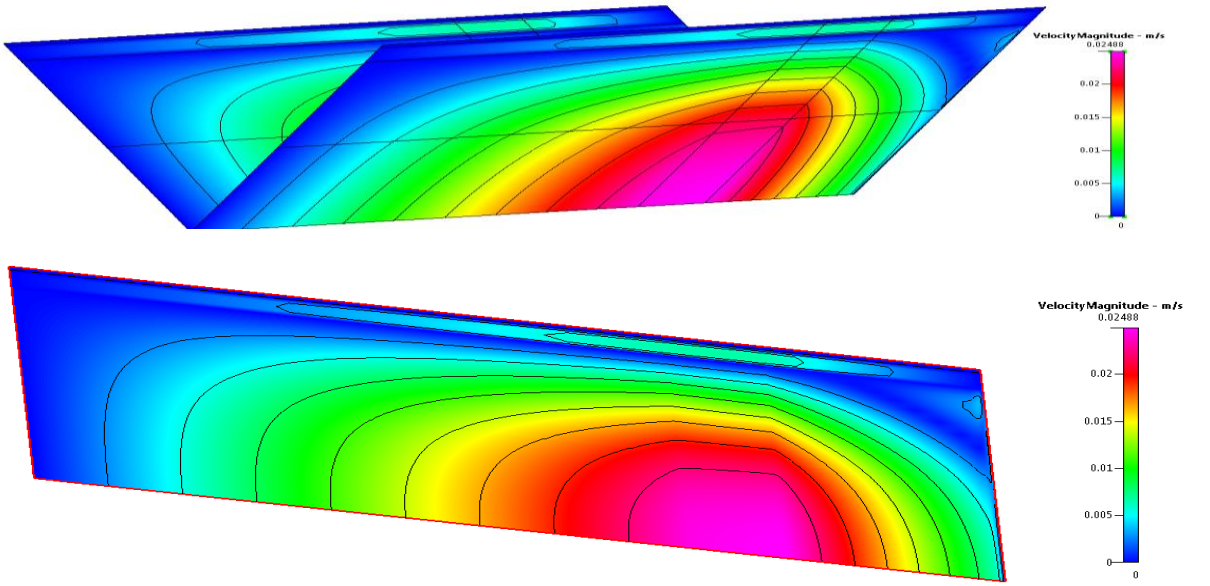

(a) The contour of velocity magnitude using nanofluid in symmetry and in r-z plane.

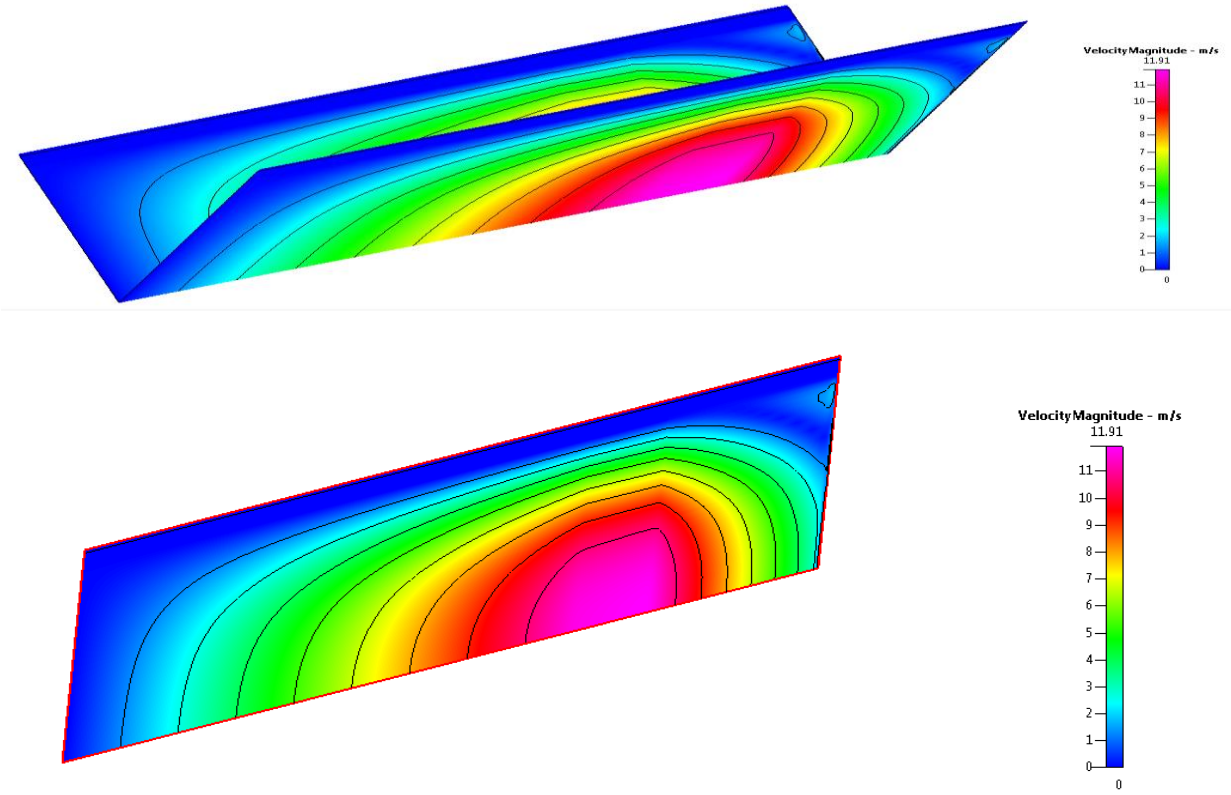

(b) The contour of velocity magnitude using pure water in symmetry and in r-z plane.

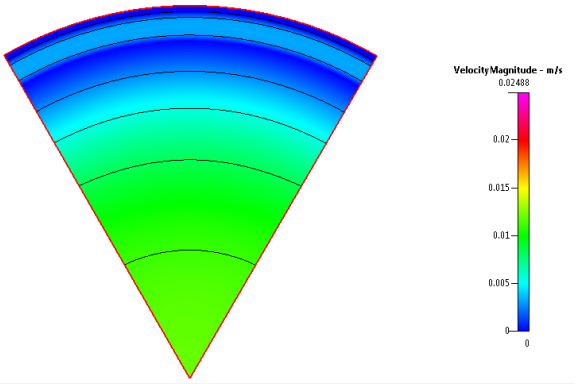

Evaporator section
(307.1 mm in axial distance from evaporator end)

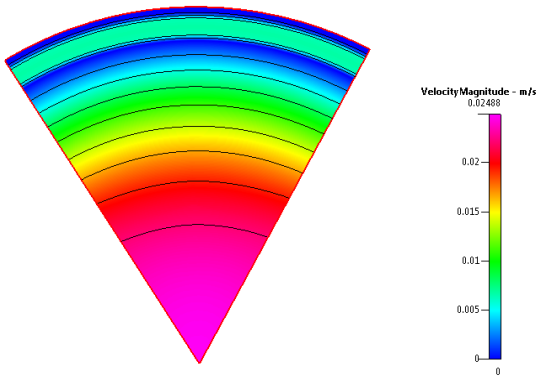

Adiabatic section
(644.4 mm in axial distance from evaporator end)

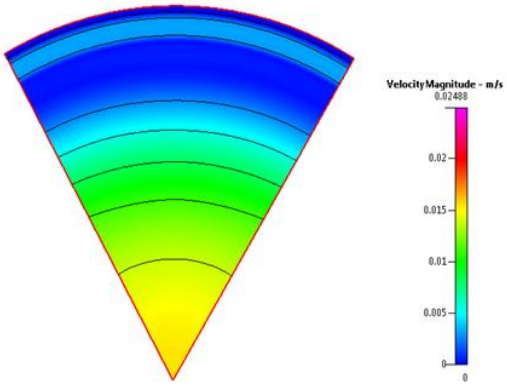

Adiabatic section
(793.9 mm in axial distance from evaporator end)

Fig. 9. The contour of velocity magnitude of Al_2O_3–water nanofluid and pure water in a cylindrical heat pipe.

The results of this study indicates that the proposed model using the viscosity and density of the Brinkman and Pak and Cho models and thermal conductivity model from the earlier studies [5], [6], [8]-[10] can be used to show the axial outer wall temperature profile, centerline velocity magnitude, centerline pressure and thermal resistance of cylindrical heat pipe in circumferential heat. The proposed model also shows that the thermal resistance of the Al_2O_3-water nanofluid cylindrical heat pipe has lower thermal resistance compared to water cylindrical heat pipe. However, the thermal conductivity models from the earlier studies [5], [6], [8]-[10] give different results of the axial outer wall temperature profile, especially in the condenser section of the cylindrical heat pipe.

These models predict the outer wall temperature distribution, velocity magnitude, pressure, while the thermal performance of nanofluid cylindrical heat pipe agrees with previous study [2], [26]. It was also found that the alumina oxide in 20 nm mixed with water can decrease thermal resistance of the cylindrical heat pipe by 5.7% in Maxwell-Garnett model, 5.7% in Hamilton and Crosser model, 36% in Jang and Choi model, 3.7% in Chon *et al.* model, 12.1% in Sitprasert *et al.* model and 21.8% in Yu and Choi model reported by Shafahi *et al.* [15] compared to that of pure water. In addition, it was observed that the use of Al_2O_3-water nanofluid increases the effective thermal conductivity in all models. Besides, the evaporator and condenser heat transfer coefficients are found to increase in Maxwell-Garnett model and Hamilton and Crosser, Jang and Choi model, Sitprasert *et al.* model and Yu and Choi model compared to that of pure water.

ACKNOWLEDGEMENTS

The CFD-RC commercial software made available by Department of Mechanical Engineering, Academic Division, Chulachomklao Royal Military Academy, Maung, Nakorn-Nayok, Thailand is acknowledged and appreciated.

Narong Pooyoo is grateful to National Science and Technology Development Agency (NSTDA), Thailand for financial support to conduct this research.

NOMENCLATURE

A_i	interface area (m^2)
C_F	quadratic drag factor (-)
C_1	proportionality constant (-)
d_{bf}	diameter of the base fluid molecule (nm)
d_{np}	diameter of the nanoparticle (nm)
D_0	

d_w	wire diameter (m)
h_0	specific total enthalpy (J/kg)
$h_{fg,nf}$	bulk latent heat of evaporation of nanofluid (J/kg)
i	internal energy (kJ)
k_{eff}	effective thermal conductivity of saturated wick (W/m.K)
K	permeability (m^2)
k_l	thermal conductivity of nanofluid (W/m.K)
k_{nf}	thermal conductivity of nanofluid (W/m.K)
k_w	thermal conductivity of wick structure (W/m.K)
k_{bf}	thermal conductivity of base fluid (W/m.K)
k_{lr}	thermal conductivity of nanolayer (W/m.K)
k_{np}	thermal conductivity of nanoparticle (W/m.K)
$\dot{k}_{np}$	thermal conductivity of nanoparticle including the effect of the Kapitza resistance (W/m.K)
k_s	thermal conductivity coefficient of solid (W/m.K)
k_v	thermal conductivity coefficient of vapor (W/m.K)
k_w	thermal conductivity of wick material (W/m.K)
L_a	adiabatic length (m)
L_c	condenser length (m)
L_e	evaporator length (m)
$\dot{m}_i$	interface mass flow rate (kg/s)
$\dot{m}_{i,e}$	interface mass flow rate per radian for evaporator at liquid-vapor interface(kg/s.π)
$\dot{m}_{i,a}$	interface mass flow rate per radian for adiabatic section at liquid-vapor interface (kg/s.π)
$\dot{m}_{i,c}$	interface mass flow rate per radian for condenser at liquid-vapor interface (kg/s.π)
N	Mesh number (1/m)
n	empirical shape factor (-)
P, p	static pressure (N/m^2)
P_v	saturation vapor pressure (N/m^2)
P_s	saturation vapor pressure (N/m^2)
Pr	Prandtl number (-)
Pr_{bf}	Prandtl number of saturated base fluid (-)
Q_a	heat input at outer adiabatic section surface (W)
Q_e	heat input at outer evaporator surface (W)
Q_c	heat input at outer condenser surface (W)
$\dot{Q}_i$	heat input per second at liquid-vapor interface (W)
$\dot{Q}_{i,e}$	heat input per second at liquid-vapor interface of evaporator (W)
$\dot{Q}_{i,c}$	heat output per second at liquid-vapor interface of condenser (W)
Re_d	Reynolds number (-)
R_i	liquid-vapor interface radius (m)
r_P	the original particle radius (m)
r	radial coordinate (m)
S_a	source term in adiabatic section (W/m^3)
S_c	source term in condenser section (W/m^3)
S_e	source term in evaporator section (W/m^3)
S_h	source term for total enthalpy (W/m3)
T	temperature (K)
T_s	solid temperature (K)
T_v	vapor temperature (K)
t	nanolayer thickness (nm)
t_w	wick thickness (m)
u	circumferential angle velocity (m/s)
$\vec{V}$	velocity vector (m/s)
v_{bf}	kinematic viscosity of the base fluid (m^2/s)
V_{Br}	Brownian velocity of nanoparticles (m/s)
V_i	liquid-vapor interface velocity (m/s)
v	radial velocity (m/s)
$V_{i,a}$	interface velocity for adiabatic section at liquid-vapor interface (m/s)
$V_{i,e}$	interface velocity for evaporator at liquid-vapor interface (m/s)
$V_{i,c}$	interface velocity for condenser at liquid-vapor interface (m/s)
$V_{nf,l}$	nanofluid velocity in liquid phase (m/s)
$V_{nf,v}$	nanofluid velocity in vapor phase (m/s)
w	axial velocity (m/s)
w	nanolayer thickness (nm)
z	axial coordinate (m)

Greek Symbols

μ_{nf}	nanofluid viscosity (Pa.S)
$\mu_{nf,l}$	nanofluid viscosity in liquid phase (Pa.S)
$\mu_{nf,v}$	nanofluid viscosity in vapor phase (Pa.S)
$\emptyset$	nanoparticle concentration is $\frac{\text{Volume of nanoparticles}}{\text{Volume of nanoparticles+Volume of base fluid}}$ (% v/v)
μ_{bf}	base fluid viscosity (Pa.S)
ρ_{nf}	nanofluid density (kg/m^3)
ρ_{bf}	base fluid density (kg/m^3)
γ	ratio of nanolayer thickness and original particle radius (-)
β_0	Function in Loeng *et al.*'s model, $1+\gamma$
β_1	Function in Loeng *et al.*'s model, $1+\frac{\gamma}{2}$
$\rho_{nf,v}$	nanofluid density in vapor phase (kg/m^3)
$\rho_{nf,l}$	nanofluid density in liquid phase (kg/m^3)
Δ	delta
∇	divergent operator
ε	wick porosity (-)
θ	circumferential angle coordinate (degree)
∂	partial difference
$\frac{\partial p}{\partial t}$	static pressure gradient in time
π	pi
τ	shear stress tensor (N/m^2)

Subscripts

a	adiabatic
bf	base fluid
c	condenser
e	evaporator
eff	effective

h	total enthalpy
i	liquid-vapor interface
i,a	liquid-vapor interface for adiabatic section
i,c	liquid-vapor interface for condenser section
i,e	liquid-vapor interface for evaporator section
nf,l	nanofluid in liquid phase
nf,v	nanofluid in vapor phase
nf	nanofluid
np	nano particle
s	saturation, solid
w	wire, wick

REFERENCES

[1] Maxwell J.C., 1881. *Treatise on Electricity and Magnetism*. Oxford, UK: Clarendon Press.

[2] Hamilton R.L. and O.K. Crosser. 1962. Thermal conductivity of heterogeneous two-component systems, *Industrial Chemical Fundamental* 1(3): 187-191.

[3] Bhattachaya P., Saha S.K., Yadav A., Phelan P.E., and Parsher R.S., 2004. Brownian dynamics simulation to determine the effective thermal conductivity of nanofluids. *Journal of Applied Physics* 95: 6492-6494.

[4] Jang S.P. and S.U.S. Choi. 2007. Effects Of various parameters on nanofluid thermal conductivity. *ASME Journal of Heat Transfer* 129: 617-623.

[5] Chon C.H., Kihm K.D., Lee S.P., and Choi S.U.S., 2005. Empirical correlation fin the role of temperature and particle size for nanofluid (Al_2O_3) thermal conductivity enhancement, *Applied Physics Letters* 87: 153107.

[6] Sitprasert C., Dechaumphai P., and Juntrasaro V., 2009. A thermal conductivity model for nanofluids including effect of the temperature -dependent interfacial layer. *Nanoparticles Research* 11: 1465-1476.

[7] Choi J. and Y. Zhang. 2012. Numerical simulation of laminar forced convection heat transfer of Al_2O_3-water nanofluid in a pipe with return bend. *International Journal of Thermal Sciences* 55: 90-102.

[8] Mahmoodi M., 2011. Numerical simulation of free convection of a nanofluid in L-shaped cavities *International Journal of Thermal Sciences* 50: 1731-1742.

[9] Do K.H. and S.P. Jang. 2010. Effect of nanofluids on the thermal performance of a flat micro heat pipe with a rectangular grooved wick. *International Journal of Heat and Mass Transfer* 53: 2183-2192.

[10] Einstein A., 1906. A new determination of the molecular dimensions. *Ann Physics* 19: 289-306.

[11] Smith J.M., and van Ness H.C., 1987. *Introduction to Chemical Engineering Thermodynamics*, McGraw-Hill, New York.

[12] Kaviany M., 1995. *Principle Of Heat Transfer In Porous Media, Second Edition*. Springer, New York.

[13] Mousa M.G, 2011. Effect of nanofluid concentration on the performance of circular heat pipe. *Ain Shams Engineering Journal* 2: 63-69.

[14] Das S.K., Choi S.U.S., Yu W., and Pradeep T., 2007. *Nanofluid Science and Technology*. London, Wiley-Interscience.

[15] Shafahi M., Bianco V., Vafai K., and Manca O., 2010, An investigation of the thermal performance of cylindrical heat pipes using nanofluids. *International Journal of Heat and Mass Transfer* 53: 376-383.

[16] Zhu N. and K. Vafai. 1999. Analysis of cylindrical heat pipe incorporating the effects of liquid-vapor coupling and non-Darcian transport a closed form solution. *International Journal of Heat and Mass Transfer* 42: 3405-3418.

[17] Huang L., EI-Genk M.S., and Tournier J.M., 1993. Transient performance of an inclined water heat pipe with a screen wick. *Heat Pipes and Capillary Pumped Loops*. 236: 87-92.

[18] Kavusi H. and D. Toghraie. 2017. A comprehensive study of the performance of a heat pipe by using of various nanofluids. *Advanced Powder Technology* 28: 3074-3084.

[19] Pak B.C., and Y.I. Cho. 1998. Hydrodynamic and heat transfer study of dispersed fluids with submicron metallic oxide particles. *Experimental Heat Transfer* 11: 151-170.

[20] Brinkman H.C., 1952. The viscosity of concentrated suspensions and solution. *Journal of Chemical Physics* 20(4): 571-581.

[21] Chi S.W., 1976. *Heat Pipe Theory and Practice*, Hemisphere, Washington, DC.

[22] Yu W. and S.U.S. Choi. 2003. The role of interfacial layers in the enhanced thermal conductivity of nanofluids: a renovated Maxwell model. *Journal of Nanoparticle Research*, 5: 167-171.

[23] Alizad K., Vafai K., and Shafahi M., 2012. Thermal performance and operational attributes of the startup characteristics of flat-shaped heat pipes using nanofluids. *International Journal of Heat and Mass Transfer* 55: 140-155.

[24] Dunn P.D. and D.A. Reay. 2005. *Heat Pipes, Theory Design and Applications*. Pergamon, New York.

[25] Shafahi M., Bianco V., Vafai K., and Manca O., 2010. Thermal performance of flat-shaped heat pipe using nanofluids. *International Journal of Heat and Mass Transfer* 53: 1438-1445.

[26] Gavtash B., Hussain K., Layeghi M., and Lafmejani S.S., 2012. Numerical simulation of the effect of nanofluid on a heat pipe thermal performance. *World Academy of Science. Engineering and Technology* 68: 549-555.

[27] Mashaei P.R., Shahryari M., Fazeli H., and Hosseinalipour S.M., 2016. Numerical Simulation of nanofluid application in a horizontal mesh heat pipe with multiple heat source: a smart fluid for high efficiency thermal system. applied thermal engineering 100: 1016-1030.

[28] Poplaski L.M, Benn S.P., and Faghri A., 2017. Thermal performance of heat pipes using nanofluids. *International Journal of Heat Mass Transfer* 107: 358-371.

[29] Herrera B., Chejne F., Mantelli M.B.H, Mejia J., and Cocoa K, 2019. Population balance for capillary limit modeling in a screen mesh wick heat pipe working with nanofluids. *International Journal of Thermal Sciences* 138: 134-158.

[30] Maddaha H., Ghazvinib M., and Ahmadic M.H, 2019. Predicting the efficiency of CuO/water nanofluid in heat pipe heat exchanger using neural network. *International Communication in Heat and Mass Transfer* 104: 33-40.

[31] Hassan H., and Harmand S., 2013. 3D Transient model of vapour chamber: effect of nanofluids on its performance. *Applied Thermal Engineering* 51: 1191-1201.

[32] Pooyoo N., Kumar S., Charoensuk J., and Suksangpanomrung A., 2014. Numerical simulation of cylindrical heat pipe considering non-Darcian transport for liquid flow inside wick and mass flow rate at liquid-vapor interface. *International Journal of Heat and Mass Transfer* 70: 965–978.

[33] Sajid M.U. and S.H.M. Ali. 2019. Recent advances in application of nanofluids in heat transfer devices: a critical review. *Renewable and Sustainable Energy Reviews* 103: 556–592.

[34] Wang C.Y. and P. Cheng. 1997. Multiphase flow and heat transfer in porous media. *Advances in Heat Transfer* 30: 93–182.

[35] CFD-ACE+ V2009 User Manual, 2009. ESI Group CFD, Incorporation, Atlanta, Georgia.

[36] Xuan Y. and W. Roetzel. 2000. Conceptions for heat transfer correlation of nanofluids. *International Journal of Heat and Mass Transfer* 43: 3701-3707.

[37] Leong K.C., Yang C., and Murshed S.M.S., 2006. A model for the thermal conductivity of nanofluids: the effect of inertial layer. *Journal of Nanoparticles Research* 8: 245-254.

[38] Faghri A., 1991. Analysis of frozen startup of high temperature heat pipes and three-dimensional modeling. Interim Report for Period January 1990-May 1991. Aero Propulsion and Power directorate, Wright Laboratory.

[39] Shabgard H. and A. Faghri. 2011. Performance characteristics of cylindrical heat pipes with multiple heat sources. *Applied Thermal Engineering* 31: 3410-3418.

[40] Aghvami M. and A. Faghri. 2011. Analysis of flat heat pipes with various heating and cooling configurations. *Applied Thermal Engineering* 31: 2645-2655.

[41] Nouri-Borujerdi A. and M. Layeghi. 2004. A numerical analysis of vapor flow in concentric annular heat pipes. *Journal of Fluid Engineering.* 126: 442-448.

[42] Mahjoub S. and A. Mahtabrosham. 2008. Numerical simulation of a convectional heat pipe, *Proceeding of World Academy of Science, Engineering Technology* 29: 117-122.

[43] Thuchayapong N., Nakano A., Sakulchangsatjatai P., and Terdtoon P., 2012. Effect of capillary pressure on performance of a heat pipe: numerical approach with FEM, *Applied Thermal Engineering* 32: 93-99.

[44] Layeghi M. and A. Nouri-Borujerdi. 2005. Vapor flow analysis in partially heated concentric annular heat pipes. *International Journal of Computational Engineering Science* 5:235–244.

[45] Nouri-Borujerdi A. and M. Layeghi. 2005. Liquid flow analysis in concentric annular heat pipe wicks. *Journal of Porous Media* 8: 471–480.

[46] Annamalai A.S. and V. Ramalingam. 2011. Experimental investigation and CFD analysis of an air-cooled condenser heat pipe. *Thermal Science* 15: 757-772.

[47] Kuzetzov G.V. and A.E. Sitnikov. 2002. Numerical modeling of heat and mass transfer in a low-temperature heat pipe. *Journal of Engineering Physics and Thermophysics* 75: 840-848.

[48] Kaya T. and J. Goldak. 2007. Three-dimensional numerical analysis of heat and mass transfer in heat pipe. *Heat and Mass Transfer* 43: 775-785.

[49] de Ornelas S., de Sousa S., Dong C., Fernelius M., Hofer M., Holsclaw T., Jennison A., Mai D., Ninh K., and van der Poel M., 2006. *Mathematical modeling, numerical simulation, and statistical optimization of heat pipe design.* Center for Applied Mathematics, Computation and Statistics, Department of Mathematics San Jose State University San Jose, CA.

[50] Mistry P.R., Thakkar F.M., De S., and Das Gupta S., 2010. Indirect experimental validation of a two-dimensional model of the transient and steady-state characteristics of a wicked heat pipe. *Experimental Heat Transfer* 23: 333–348.

[51] Ergun S., 2007. Fluid flow through packed columns. *Chemical Engineering Program*. 48: 89–90.

[52] Versteeg H.K. and W. Malasekera. 2007. *An Introduction to Computational Fluid Dynamics, The Finite Volume Method*. Pearson, Prentice Hall.

[53] Peterson G.P., 1994. *Heat Pipes: Modeling, Testing and Applications*. John Willey & Sons, Incorporation, United States of America.

[54] Schmalhofer J. and A. Faghri. 1993. A study of circumferentially heated and block-heated heat pipes-ii, three-dimensional modeling as a conjugate problem. *International Journal of Heat and Mass Transfer* 36: 213-226.

[55] Brusly S.A., Ramachandran K., Godson A.L., and Pillai B.C., 2014 Numerical analysis of a screen mesh wick heat pipe with Cu/water. *International Journal of Heat and Mass Transfer* 75: 523-533.